Available online at www.sciencedirect.com
ScienceDirect
Journal of Sound and Vibration 314 (2008) 70–82
JOURNAL OF SOUND AND VIBRATION
www.elsevier.com/locate/jsvi

Damping of elastic strain waves by means of a piezoelectric bar element feeding an external RL circuit

A. Jansson, B. Lundberg*

The Ångström Laboratory, Uppsala University, Box 534, SE-751 21 Uppsala, Sweden

Received 23 August 2007; received in revised form 19 December 2007; accepted 25 December 2007
Handling Editor: A.V. Metrikine
Available online 21 February 2008

Abstract

Damping of elastic strain waves in an aluminum bar by means of a pair of piezoelectric members bonded to the bar and loaded by an external RL circuit is studied. Experimental results are compared with theoretical results based on a three-port impedance model for the laminated piezoelectric bar element (PBE). According to this model, the PBE is viewed as a linear system with one electrical and two mechanical ports at which interactions with external devices, e.g., the external parts of the aluminum bar, can take place. The two constitutive equations of the piezoelectric material, the dynamics of the piezoelectric members and the bar, and the dynamics of the resistive-inductive load are taken into account. The experimental results are below the theoretical ones by a few percent for the reflected and transmitted strain waves, by 6–11% for the voltage and current generated, and by 12–19% for the power and energy delivered to the load. This indicates that there are energy losses in the PBE and the external parts of the bars that have not been accounted for in the model. Such losses may be due to, e.g., viscoelastic shear, dielectric losses and generation of bending waves.

1. Introduction

Piezoelectric members in the form of thin plates, covered with conducting electrode layers, are increasingly used as sensors, e.g. Refs. [1,2], and actuators, e.g. Refs. [3,4] in various applications. Their ability of producing electrical output when subjected to mechanical input and vice versa originate from two coupled constitutive equations [5], the sensor and actuator equations, that relate the mechanical and electrical fields in piezoelectric materials. In addition to these equations, analyses of piezoelectric members interacting with mechanical and electrical devices generally involve the dynamics of the piezoelectric members as well as of the mechanical and electrical devices.

Early work on piezoelectric actuation was carried out by Crawley and de Luis [6]. Actuator dynamics was taken into account by, e.g., Pan et al. [7] for the system of a beam with attached piezoelectric actuators. Allowance for the two constitutive equations, and the interaction of structure and electrical circuits, was made by, e.g., Hagood et al. [8], Thornburgh and Chattopadhyay [9], and Thornburgh et al. [10].

*Corresponding author.
E-mail address: bengt.lundberg@angstrom.uu.se (B. Lundberg).

0022-460X/$ - see front matter © 2008 Elsevier Ltd. All rights reserved.
doi:10.1016/j.jsv.2007.12.033

Nomenclature

Latin letters

A	cross-sectional area
c	wave speed
C	capacitance
d	piezoelectric constant
e	strain
E	Young's modulus
f	frequency
h	height
i	current
k	square root of piezoelectric coupling coefficient
K	stiffness
l	length
L	inductance
N	normal force
R	real part of impedance, resistance
t	time
U	voltage
v	particle velocity
w	width, normalized energy
W	energy
x	axial coordinate
y	transverse coordinate (horizontal)
z	transverse coordinate (vertical)
Z	impedance (mechanical, electrical or mixed)

Greek letters

γ	wave propagation coefficient
ε	permittivity
ρ	density
ω	angular frequency

Superscripts

E	electrical
M	mechanical

Subscripts

0	electrical port
1	1st mechanical port
2	2nd mechanical port
a	piezoelectric layer
c	core layer
ch	characteristic
D	dissipated
I	incident
int	internal
L	loss
R	reflected
tr	transit
T	transmitted

The possibility of using piezoelectric elements with passive electrical shunts for vibration damping and control was first suggested by Forward [11]. Subsequent work along these lines has been carried out by, e.g., Hagood and von Flotow [12], Fein and Gaul [13], and Panella and Martinelli [14]. Progress in damping and control by use of shunted piezoelectric transducers can be found in surveys by Lesieutre [15], Tang et al. [16], and Moheimani [17]. A recent general overview of research in the area of smart structure dynamics, addressing also the use of chemo-mechanical materials and shape memory alloys, has been provided by Hurlebaus and Gaul [18].

While there is much published work on piezoelectricity related to vibrations of beams, there is only little such work related to transient extensional strain waves in bars. In a paper by the authors [19], a straight bar element containing piezoelectric members is viewed as a linear system with one electrical and two mechanical interfaces or ports at which interactions with external devices can take place. These interactions are described in terms of voltage, current, forces, and velocities. One voltage and the two forces constitute generalized forces, and one current and the two velocities form generalized velocities. The vector of generalized forces is expressed as the product of an impedance matrix and the vector of generalized velocities. Due to symmetry and reciprocity, this impedance matrix is defined by four of its nine elements. With these impedance elements known, the function of the piezoelectric bar element (PBE) in different applications can be analyzed. In particular, the applications of strain wave generation and damping are considered for a laminated PBE consisting of an elastic core and a pair of piezoelectric members bonded to the core. In the first of these applications, the laminated PBE is driven by a linear power amplifier, and in the second it feeds an external

load impedance. The two constitutive equations, the dynamics of the piezoelectric members and the bar, and the dynamics of the amplifier and the load impedance are taken into account.

For strain wave generation, with electrical input and mechanical output, good agreement has been achieved between theoretical and experimental results for the waves generated by use of the laminated PBE [20]. For strain wave damping, however, with mechanical input and electrical output, corresponding published experimental results have not been found. For this case, therefore, an experimental study has been carried out with a long aluminium bar, a laminated PBE, constituted by a part of the bar with a pair of attached piezoelectric members, and a load impedance consisting of an RL circuit. The primary aim was to validate the laminated PBE model by comparing theoretical and experimental results for the reflected and transmitted strain waves, the generated voltage and current, and the power and energy delivered to the load. A secondary aim was to study how the dissipated energy depends, in rather limited ranges, on the resistance and inductance of the load.

The theoretical background, based on the three-port impedance model of the PBE, will be presented next. The experimental setup and procedure will be described in Section 3. The theoretical and experimental results will be presented and discussed in Section 4, and main conclusions will be summarized in Section 5.

2. Theoretical background

Consider the electromechanical system in Fig. 1(a) consisting of a long elastic bar with a pair of attached piezoelectric members a shunted by an external load impedance Z_0. The length of the laminated region $-l/2<x<l/2$, i.e., the laminated PBE, is l, where x is an axial coordinate as shown. An incident strain wave associated with the normal force $\hat{N}_I(\omega)$ at $x=-l/2$ is assumed to generate reflected and transmitted strain waves associated with the normal forces $\hat{N}_R(\omega)$ at $x=-l/2$ and $\hat{N}_T(\omega)$ at $x=l/2$, respectively, and a voltage $\hat{U}_0(\omega)$ driving a current $-\hat{i}_0(\omega)$ through the external load impedance. Here and below, ω is the angular frequency, and the notation $\hat{\phi}(\omega)$ is used for the Fourier transform of a function $\phi(t)$ of time t assumed to be piecewise differentiable and absolutely integrable.

Thin bonding layers are assumed to have no other effect than perfectly attaching the piezoelectric members to the bar. The cross-sections of the bar and the piezoelectric members are rectangular, and the full cross-sections inside and outside the laminated region are symmetric with respect to the y and z axes. Outside the laminated region, the bar has height h_1, width w_1 and cross-sectional area $A_1=h_1w_1$. In the core c of the laminated region, it has height h_c, width w_c, and cross-sectional area $A_c=h_cw_c$. Each piezoelectric member has height h_a, width w_a, and cross-sectional area $A_a=h_aw_a$. Therefore, the total cross-sectional area of the laminated PBE is $A=2A_a+A_c$.

The Young's modulus of the bar material is assumed to be E_1, while that of the piezoelectric members, when short-circuited, is assumed to be E_a. The densities are assumed to be ρ_1 and ρ_a, respectively. Further, it is assumed that initially plane cross-sections remain plane and that the stress is uni-axial. Within the PBE, therefore, the effective Young's modulus is $E=(2A_aE_a+A_cE_c)/A$, with $E_c=E_1$, and the effective density is $\rho=(2A_a\rho_a+A_c\rho_c)/A$, with $\rho_c=\rho_1$. The wave speeds in the bar and the PBE are $c_1=(E_1/\rho_1)^{1/2}$ and $c=(E/\rho)^{1/2}$, and the characteristic impedances are $Z_1=A_1E_1/c_1$ and $Z_{\mathrm{ch}}^M=AE/c$, respectively.

The piezoelectric material is assumed to be polarized in the z direction and to have linear electromechanical response. In addition to the closed-circuit Young's modulus E_a, this response is characterized by the permittivity ε_a and the piezoelectric constant $d_a=-d_{31}$. The electrical fields between the electrode layers on the upper and lower faces of the actuators are assumed to be parallel to the z-axis, and the effects of strains in the y and z directions are neglected.

The PBE viewed as a three-port electromechanical linear system [19] is shown in Fig. 1(b). The piezoelectric members, connected symmetrically in parallel, feed the external load impedance at a single port labeled 0, where the voltage is $\hat{U}_0(\omega)$ and the current is $\hat{i}_0(\omega)$. The current is defined as positive in the direction it would be driven through the port by a positive voltage from an external source. The PBE interacts with the external parts of the bar at the two interfaces or ports labeled 1 and 2, constituted by its ends, where the normal forces are $\hat{N}_1(\omega)$ and $\hat{N}_2(\omega)$, and the particle velocities are $\hat{v}_1(\omega)$ and $\hat{v}_2(\omega)$. The forces are defined as positive in tension and the velocities in the direction of the x-axis.

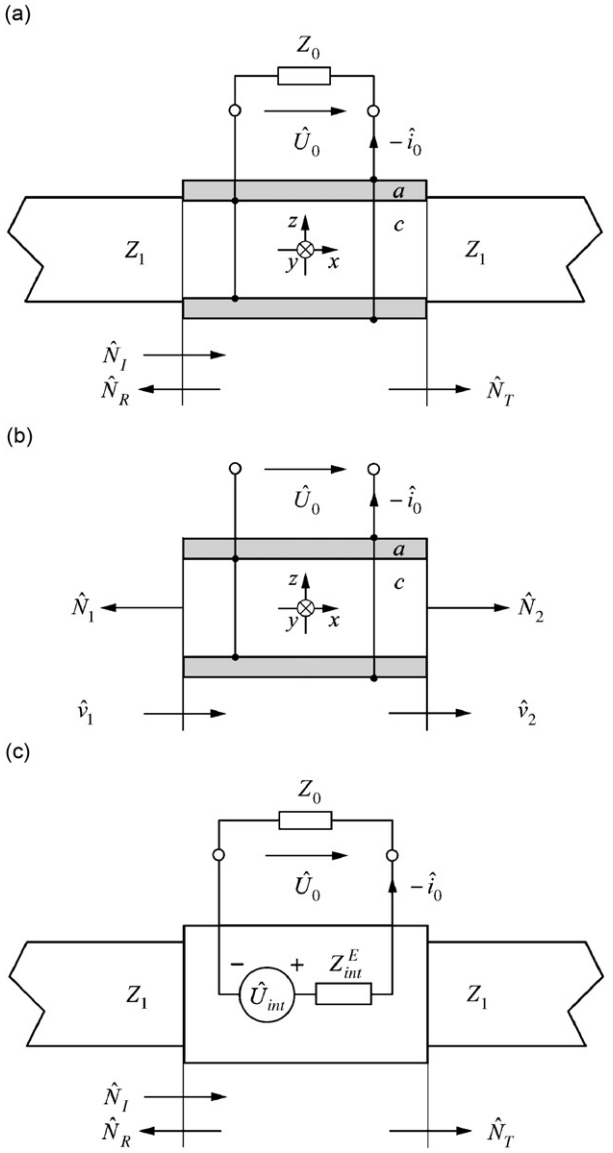

Fig. 1. Electromechanical system. (a) Elastic bar with attached piezoelectric members and external load impedance. (b) Three-port representation of laminated PBE. (c) Equivalent electrical circuit.

Due to linearity, the generalized forces $\hat{U}_0$, $\hat{N}_1$, $\hat{N}_2$ are related to the generalized velocities $\hat{i}_0$, $-\hat{v}_1$, $\hat{v}_2$ by the system [19]

$$\hat{U}_0 = Z_{00}\hat{i}_0 + Z_{01}(-\hat{v}_1) + Z_{02}\hat{v}_2, \tag{1a}$$

$$\hat{N}_1 = Z_{10}\hat{i}_0 + Z_{11}(-\hat{v}_1) + Z_{12}\hat{v}_2, \tag{1b}$$

$$\hat{N}_2 = Z_{20}\hat{i}_0 + Z_{21}(-\hat{v}_1) + Z_{22}\hat{v}_2, \tag{1c}$$

where $Z_{00}(\omega)$, $Z_{01}(\omega)$, …, $Z_{22}(\omega)$ are impedances. Because of reciprocity and the symmetry with respect to the yz plane, this system is defined by the four impedances Z_{00}, Z_{01} ($= Z_{10} = Z_{02} = Z_{20}$), Z_{11} ($= Z_{22}$), and

Z_{12} ($=Z_{21}$). For the laminated PBE considered here, these impedances are [19]

$$Z_{00}=\frac{1}{2}\frac{Z_a^E}{1-k_a^2},\quad Z_{01}=\frac{d_a h_a}{\varepsilon_a A_a}\frac{Z_a^M}{1-k_a^2}=A_a E_a\frac{d_a}{h_a}\frac{Z_a^E}{1-k_a^2}, \tag{2a, b}$$

$$Z_{11}=2\frac{k_a^2 Z_a^M}{1-k_a^2}+\frac{Z_{\mathrm{ch}}^M}{\tanh(\gamma l)},\quad Z_{12}=2\frac{k_a^2 Z_a^M}{1-k_a^2}+\frac{Z_{\mathrm{ch}}^M}{\sinh(\gamma l)}. \tag{2c, d}$$

Here $Z_a^E=1/\mathrm{i}\omega C_a$ is the electrical impedance of a single mechanically unloaded piezoelectric member with capacitance $C_a=\varepsilon_a w_a l/h_a$, $Z_a^M=K_a/\mathrm{i}\omega$ is the quasi-static mechanical impedance of a single electrically short-circuited piezoelectric member with stiffness $K_a=A_a E_a/l$, $k_a^2=d_a^2 E_a/\varepsilon_a$ is the piezoelectric coupling coefficient, and $\gamma=\mathrm{i}\omega/c$ is the wave propagation coefficient.

Continuity of forces and velocities give $\hat{N}_1=\hat{N}_I+\hat{N}_R$ and $\hat{v}_1=(1/Z_1)(-\hat{N}_I+\hat{N}_R)$ at the first mechanical port, and $\hat{N}_2=\hat{N}_T$ and $\hat{v}_2=-(1/Z_2)\hat{N}_T$ at the second. At the electrical port, the voltage is related to the current by $\hat{U}_0=Z_0(-\hat{i}_0)$. These five relations and the three equations (1) constitute a linear system of eight independent equations for the eight unknowns $\hat{i}_0$, $\hat{v}_1$, $\hat{v}_2$, $\hat{U}_0$, $\hat{N}_1$, $\hat{N}_2$, $\hat{N}_R$, and $\hat{N}_T$. Solving for the waves, the voltage and the current gives

$$\hat{N}_R=\frac{(Z_{11}^2-Z_{12}^2-Z_1^2)(Z_{00}+Z_0)-2Z_{01}^2(Z_{11}-Z_{12})}{((Z_{11}+Z_1)^2-Z_{12}^2)(Z_{00}+Z_0)-2Z_{01}^2(Z_{11}-Z_{12}+Z_1)}\hat{N}_I, \tag{3a}$$

$$\hat{N}_T=\frac{2Z_1(Z_{12}(Z_{00}+Z_0)-Z_{01}^2)}{((Z_{11}+Z_1)^2-Z_{12}^2)(Z_{00}+Z_0)-2Z_{01}^2(Z_{11}-Z_{12}+Z_1)}\hat{N}_I, \tag{3b}$$

$$\hat{U}_0=\frac{2Z_{01}Z_0}{(Z_{11}+Z_{12}+Z_1)(Z_{00}+Z_0)-2Z_{01}^2}\hat{N}_I, \tag{3c}$$

$$-\hat{i}_0=\frac{2Z_{01}}{(Z_{11}+Z_{12}+Z_1)(Z_{00}+Z_0)-2Z_{01}^2}\hat{N}_I. \tag{3d}$$

From the last two of these equations it has been shown [19] that the external load can be considered to be fed by the internal voltage

$$\hat{U}_{\mathrm{int}}=\frac{2Z_{01}}{Z_{11}+Z_{12}+Z_1}\hat{N}_I \tag{4}$$

through the internal impedance

$$Z_{\mathrm{int}}^E=Z_{00}-\frac{2Z_{01}^2}{Z_{11}+Z_{12}+Z_1} \tag{5}$$

as illustrated by the equivalent circuit of Fig. 1(c).

The energies associated with the incident, reflected, and transmitted waves are

$$W_I=\frac{1}{Z_1}\int_0^\infty N_I^2(t)\,\mathrm{d}t,\quad W_R=\frac{1}{Z_1}\int_0^\infty N_R^2(t)\,\mathrm{d}t,\quad W_T=\frac{1}{Z_1}\int_0^\infty N_T^2(t)\,\mathrm{d}t, \tag{6a–c}$$

respectively, and the power and energy delivered to the external load at time t are

$$P_0=U_0(-i_0),\quad W_0=\int_0^t P_0\,\mathrm{d}\tau. \tag{7a, b}$$

The energy finally dissipated in the external load is $W_D=W_0(\infty)$, and the relative energy dissipation is defined as

$$w_D=\frac{W_D}{W_I}. \tag{8}$$

In the above results, the forces $\hat{N} = \hat{N}_I$, $\hat{N}_R$, and $\hat{N}_T$ can be expressed in terms of the corresponding strains $\hat{e} = \hat{e}_I$, $\hat{e}_R$, and $\hat{e}_T$ by substituting $\hat{N} = Z_1 c_1 \hat{e}$ (subscripts I, R and T left out).

3. Experimental setup and procedure

The experimental setup is shown in Fig. 2.

An aluminium bar with length 3.00 m, height $h_1 = 4.0$ mm, and width $w_1 = 4.0$ mm was used. Within the PBE, the bar was milled symmetrically from two opposite sides over the length 95.4 mm to height $h_c = 3.4$ mm, while its width $w_c = w_1 = 4.0$ mm was left the same as in the rest of the bar. The material of the bar had Young's modulus $E_1 = 69$ GPa and density $\rho_1 = 2700\,\mathrm{kg/m^3}$.

In each milled slot, three piezoelectric plates (Piezo Systems, Inc., T226-A4-203Y, ceramic type 5A4E) with length 31.8 mm, height $h_a = 0.66$ mm, and width $w_a = 6.4$ mm were bonded in mechanical contact with each other, and connected electrically in parallel, so that they formed a piezoelectric member with length $l = 95.4$ mm. An epoxy adhesive (Loctite 3430) was used as bonding material, and care was taken to achieve very thin bonding layers (estimated thickness about 0.03 mm). The piezoelectric material of the plates had closed-circuit Young's modulus $E_a = 66$ GPa, density $\rho_a = 7800\,\mathrm{kg/m^3}$, permittivity $\varepsilon_a = 1.6 \times 10^{-8}\,\mathrm{A\,s/V\,m}$ and piezoelectric constant $d_a = -d_{31} = 190 \times 10^{-12}\,\mathrm{m/V}$.

The dimensions and material properties of the PBE-bar assembly correspond to parameters as follows: wave speed $c_1 = 5050$ m/s in the bar and $c = 3800$ m/s in the PBE, transit time for a wave through the PBE $t_{\mathrm{tr}} = 25.0\,\mu\mathrm{s}$, characteristic impedance $Z_1 = 219\,\mathrm{N\,s/m}$ in the bar and $Z_{\mathrm{ch}}^M = 392\,\mathrm{Ns/m}$ in the PBE, capacitance of an unloaded compound piezoelectric plate $C_a = 14.7$ nF, and the piezoelectric coupling coefficient $k^2 = 0.150$.

The bar rested horizontally on supports covered with Teflon layers in order to reduce friction. It was axially impacted at one end. The striker was made of the same material and had the same square cross-section as the bar, and its length was 50 mm. The impact face was flat except at its four edges, which were slightly rounded. It was accelerated by means of a spring and accurately guided in order to avoid generation of bending waves. As a result of impact, a strain pulse with approximate length 100 mm and duration 20 μs was generated in the bar.

A resistor R_0 in series with an inductor L_0 constituted the external load $Z_0 = R_0 + \mathrm{i}\omega L_0$. Three different inductors were used, each of them with seven different resistors. Each of these resistors was connected in series with a resistor of 4.2 Ω used to determine the current through the load. The measured total resistances of the series combinations of the two resistors, the inductor and the cables were (1) $R_0 = 54.4$, 154, 204, 304, 403, 502, and 1490 Ω for $L_0 = 0$, (2) $R_0 = 56.6$, 156, 205, 305, 404, 503, and 1491 Ω for $L_0 = 480\,\mu\mathrm{H}$, and

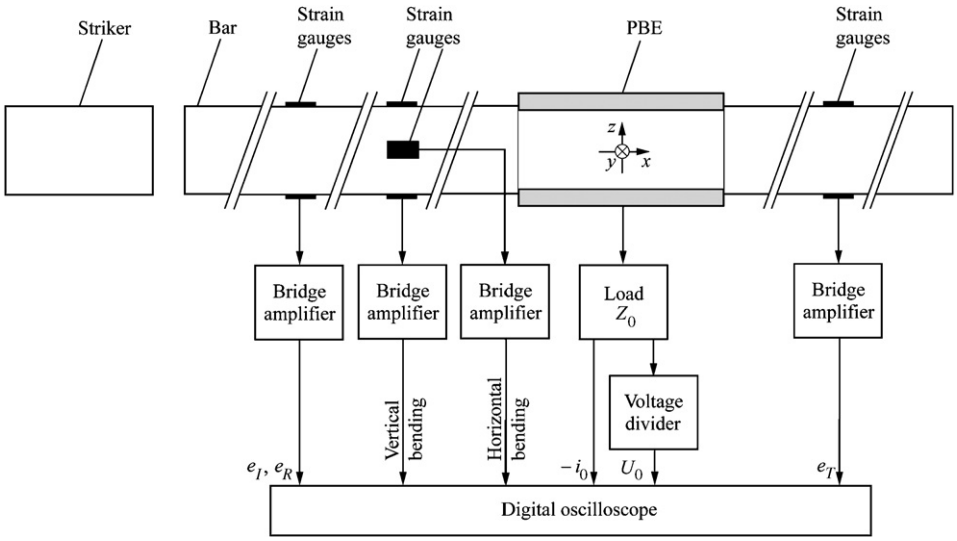

Fig. 2. Experimental setup.

Table 1
Three cases of external load impedance $Z_0 = R_0 + i\omega L_0$

Case	Inductance L_0 (μH)	Resistance R_0 (Ω)
1	0	403
2	480	305
3	1050	206

(3) $R_0 = 57.1$, 156, 206, 306, 405, 505 and 1492 Ω for $L_0 = 1050$ μH. The resistances underlined and the corresponding inductances form Cases 1–3 summarized in Table 1.

On both sides of the PBE, at a distance $a = 200$ mm from each interface, the bar was instrumented with resistive strain gauge pairs (Kyowa, type KFG-02-120-C1-11L1M2R) connected to bridge amplifiers (Vishay Measurements Group, 2210) with bandwidth 100 kHz (3 dB). The connections were such that axially symmetric strains could be measured, while influence from accidental bending in the xz plane was suppressed. In addition, at a distance 100 mm from the interface on the impacted side of the PBE, the bar was instrumented with two resistive strain gauge pairs (Tokyo Sokki Kenkyujo Co. Ltd., type FLA-1-11-1L) connected to bridge amplifiers of the same type as above. The connections were such that strains due to bending in the xy and xz planes could be monitored, while influence from axially symmetric strain waves was suppressed. Shunt calibration was used for the strain measurements. The generated voltage $U_0(t)$ was reduced by a factor of 21 by means of a resistive voltage divider before it was recorded. The current $i_0(t)$ was determined from the recorded voltage across a resistor as described above.

Before the arrival of reflected waves from the ends of the bar, the strains $e'_I(t)$, $e'_R(t)$, and $e'_T(t)$ associated with the incident, reflected, and transmitted waves at the strain gauge positions, and the voltage $U_0(t)$ and current $i_0(t)$, were recorded by means of a digital oscilloscope card (UF.3122, Strategic Test Scandinavia AB). No filters were used, and the sampling rate was 10 MHz. All 21 tests were carried out at room temperature. The measured strains were referred to the PBE interfaces through the relations $e_I(t) = e'_I(t - a/c_1)$, $e_R(t) = e'_R(t + a/c_1)$, and $e_T(t) = e'_T(t + a/c_1)$.

4. Results and discussion

Theoretical and experimental results for impedances, strain waves, voltage, current, power, and energy for the three cases in Table 1 are shown in Figs. 3–6. Such results for the relative energy dissipation corresponding to the 21 cases of experimental tests are shown in Fig. 7.

The real and imaginary parts of the internal impedance Z^E_{int}, given by Eq. (5), and of the load impedance $Z_0 = R + i\omega L$ for Cases 1–3 are shown in Figs. 3(a), (c), and (e). The spectra $|\hat{U}_{\text{int}}|$ of the internal voltage given by Eq. (4) for the same cases are shown in Figs. 3(b), (d), and (f). Maximum delivery of power to the load from the incident wave through the internal source $\hat{U}_{\text{int}}$ is achieved if the load impedance Z_0 is matched to the internal impedance Z^E_{int} so that $Z_0 = \bar{Z}^E_{\text{int}}$. For given impedances, there is generally no frequency at which this matching condition is satisfied with respect to both its real part $\text{Re}(Z_0) = \text{Re}(Z^E_{\text{int}})$ and its imaginary part $\text{Im}(Z_0) = -\text{Im}(Z^E_{\text{int}})$. In the three cases considered, there is always a significant mismatch of the real parts of the impedances, while the imaginary parts are matched at very high frequencies in Case 1, at 46 kHz in Case 2 and at 31 kHz in Case 3. However, the significant frequencies of the spectra of the internal voltage $\hat{U}_{\text{int}}$ are below these frequencies.

The strains e_I, e_R, and e_T at the PBE interfaces associated with the incident, reflected, and transmitted waves are shown in Figs. 4(a), (c), and (e) for Cases 1–3. The theoretical results for the reflected and transmitted strain waves were obtained from Eqs. (3a) and (3b) with the measured incident strain wave as input. The experimental strains are translated in time by $\pm a/c_1$ as described above. There is quite a good agreement between the theoretical and experimental results; generally, the experimental strain amplitudes are a few percent lower than their theoretical counterparts. The results show that the changes in load impedance had little effect on the waves. The corresponding spectra $|\hat{e}_I|$ of the incident strain waves are shown in Figs. 4(b), (d), and (f). These spectra have significant frequencies up to about 50 kHz, corresponding to wavelengths

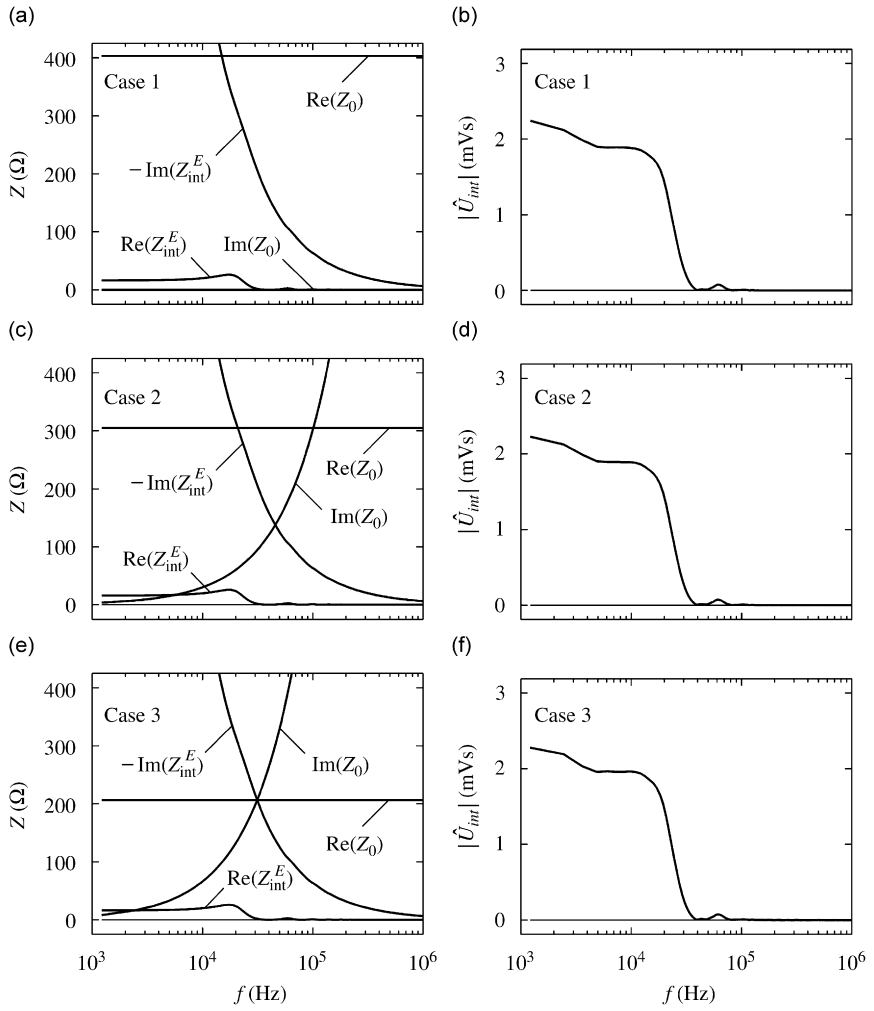

Fig. 3. Real and imaginary parts of internal impedance Z^E_{int} and of load impedance $Z_0 = R_0 + i\omega L_0$, and spectrum $|\hat{U}_{\text{int}}|$, versus frequency f. (a) Impedances and (b) spectrum for Case 1. (c) Impedances and (d) spectrum for Case 2. (e) Impedances and (f) spectrum for Case 3.

larger than about 100 mm in the bar and 76 mm in the PBE. In both cases, the wavelengths are so much larger than the transverse dimensions of the cross-sections that the one-dimensional model used should be accurate. The surface strain in the bar due to bending was less than about 5% of the maximum strain associated with the incident wave.

The voltage U_0 and current $-i_0$ generated are shown in Fig. 5 for Cases 1–3. They are of oscillatory nature with rapidly decaying tails, and they are, essentially, in phase. The theoretical results were obtained from Eqs. (3c) and (3d) with the measured incident strain wave as input. They generally agree well with the experimental results. However, the experimental voltage and current peaks are 6–11% lower than predicted by theory. The results show that the changes in load impedance had noticeable effects on the voltage and current. In particular, the relative importance of the second period of oscillation of voltage and current largely increased from Case 1 to Case 3.

The electric power P_0 and energy W_0 delivered to the load are shown in Fig. 6 for Cases 1–3. The power is oscillatory with two or three major positive peaks and one or two very small negative peaks followed by rapidly decaying tails. Correspondingly, the energy reaches an almost constant level through two or three rapid increases. Both the theoretical and the experimental results were obtained from Eqs. (7) and the results for voltage and current. There is a fair overall agreement between the theoretical and experimental results, but

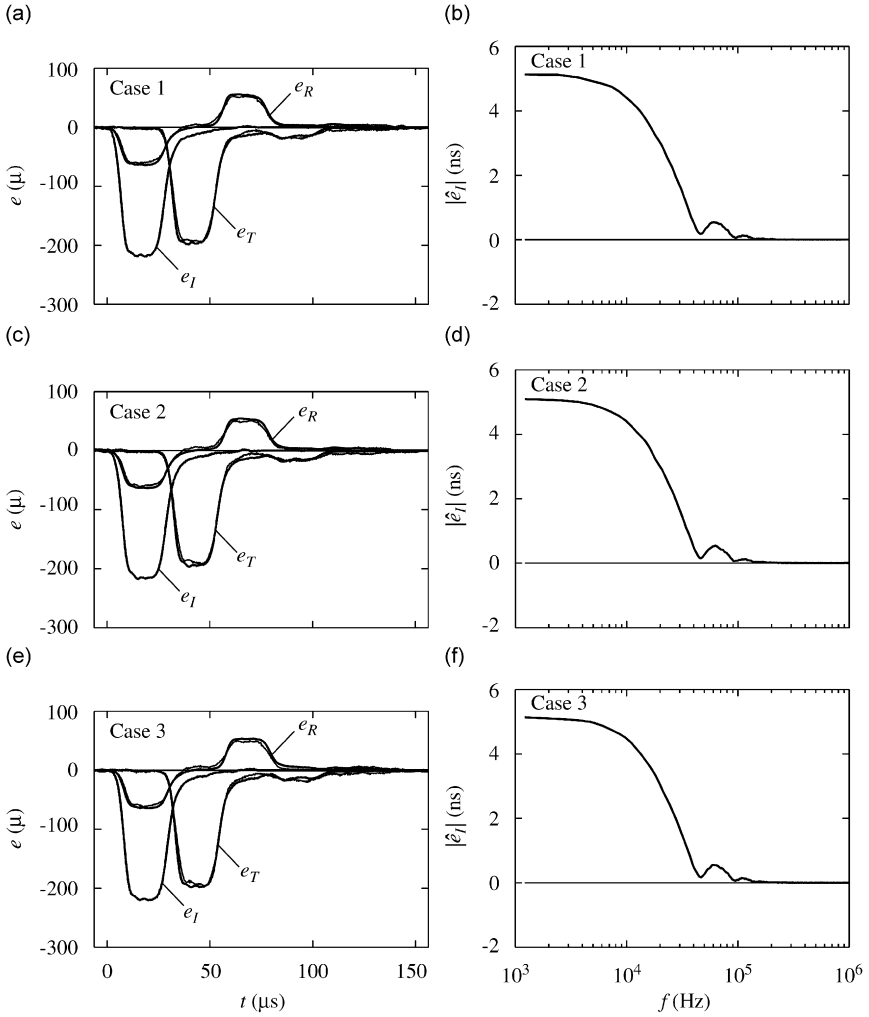

Fig. 4. Strains e_I, e_R, and e_T at PBE interfaces associated with incident, reflected and transmitted waves versus time t, and spectrum $|\hat{e}_I|$ versus frequency f, for different load impedances $Z_0 = R_0 + i\omega L_0$. (a) Strains and (b) spectrum for Case 1. (c) Strains and (d) spectrum for Case 2. (e) Strains and (f) spectrum for Case 3. Comparison between theoretical (thick curves) and experimental (thin curves) results.

the experimental power peaks and energy levels are 12–19% lower than their theoretical counterparts. Deviations of this order are in accord with the observed deviations in the voltage and current peaks. The results show that the changes in load impedance had significant effects on the power and energy delivered to the load.

The dependency of the relative energy dissipation w_D on the resistance R_0 and inductance L_0 of the load is shown in Fig. 7. Both the theoretical and experimental results were obtained from Eqs. (8) and (6a). The results for the resistances used in the experimental tests and in the theoretical calculations are marked by circles, and the resistances of Cases 1–3 are indicated by vertical lines. For each inductance L_0, w_D has a maximum with respect to the resistance R_0. The theoretical maxima of 2.7%, 3.0%, and 3.4% occur at $R_0 = 403$, 404, and 306 Ω, respectively. The corresponding experimental maxima occur at $R_0 = 403$, 305, and 206 Ω and are 15–18% lower. Because of the impedance mismatch, it was expected that the maxima are much lower than the theoretical maximum of 50% for a harmonic wave under condition of impedance matching [19].

At first sight it might seem surprising that the maxima in w_D occur at load resistances $R_0 = \mathrm{Re}(Z_0)$ that are very much larger than the resistive part $\mathrm{Re}(Z^E_{\mathrm{int}})$ of the internal impedance within the significant part of the

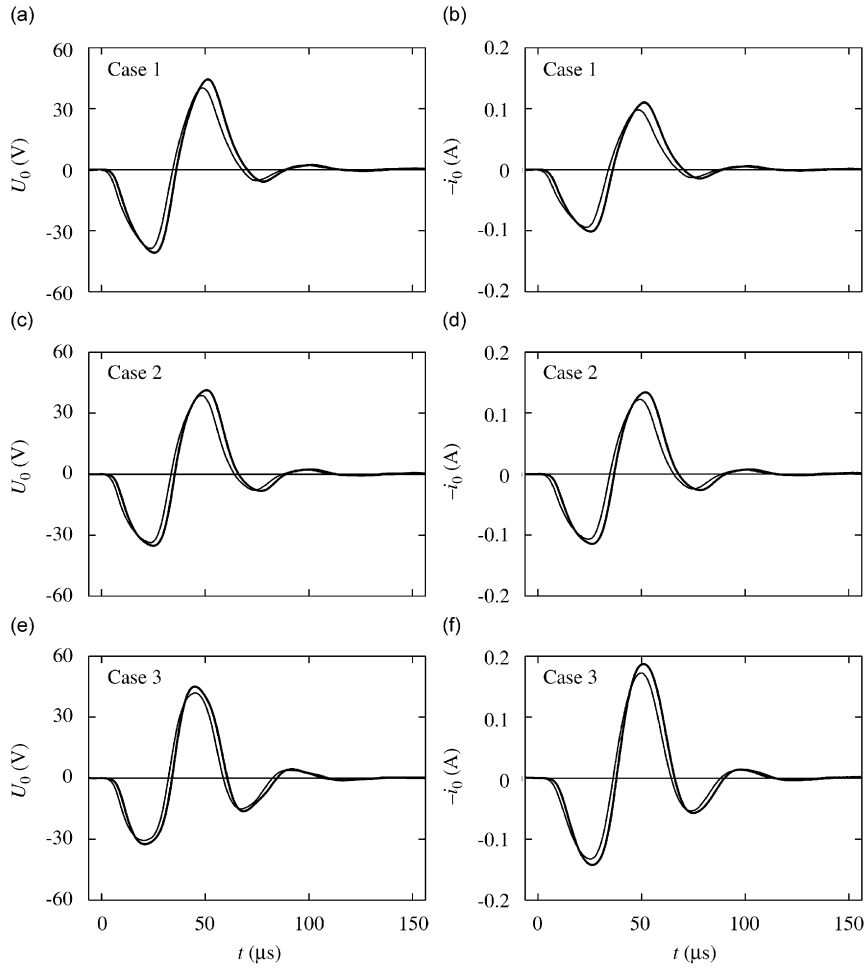

Fig. 5. Generated voltage U_0 and current $-i_0$ versus time t for different load impedances $Z_0 = R_0 + \mathrm{i}\omega L_0$. (a) Voltage and (b) current for Case 1. (c) Voltage and (d) current for Case 2. (e) Voltage and (f) current for Case 3. Comparison between theoretical (thick curves) and experimental (thin curves) results.

spectrum. The explanation is as follows: within most of this part of the spectrum, Fig. 3 shows that $\mathrm{Re}(Z^E_{\mathrm{int}})$ and $\mathrm{Im}(Z_0)$ can be neglected in comparison with $-\mathrm{Im}(Z^E_{\mathrm{int}})$. If it is assumed for a moment that these quantities can be neglected also in comparison with $R_0 = \mathrm{Re}(Z_0)$, then the internal impedance is reactive and the load is resistive. Under this condition, maximum power is delivered to the load if $R_0 = \mathrm{Re}(Z_0) = \left|\mathrm{Im}(Z^E_{\mathrm{int}})\right| \gg \mathrm{Re}(Z^E_{\mathrm{int}})$. If R_0 is much smaller than $\left|\mathrm{Im}(Z^E_{\mathrm{int}})\right|$, the voltage across the load becomes very small. If R_0 is much larger, the current through the load becomes very small. In both cases, the power and energy delivered to the load also become small.

The energy balance $W_I - (W_R + W_T + W_D) = 0$ for a lossless PBE-bar assembly is satisfied with high numerical accuracy by the theoretical results. This was to be expected as the total power supplied to the PBE at its three ports has been shown to be zero under harmonic excitation [19]. The first term of this energy balance is the same theoretically and experimentally. As evident from Figs. 4–7, however, the experimental result for each term within the parenthesis is smaller than the corresponding theoretical value. Therefore, the experimental energy balance can be written as $W_I - (W_R + W_T + W_D + W_L) = 0$, where the added term W_L represents losses in the PBE and the external parts of the bars that have not been taken into account theoretically. Such losses, estimated to be 5–10% of W_I, may be of both mechanical and electrical nature. They may be partially explained by, e.g., contributions from viscoelastic shear in the bonding layers, dielectric losses in the piezoelectric members and generation of bending waves in the external parts of the bar. It seems

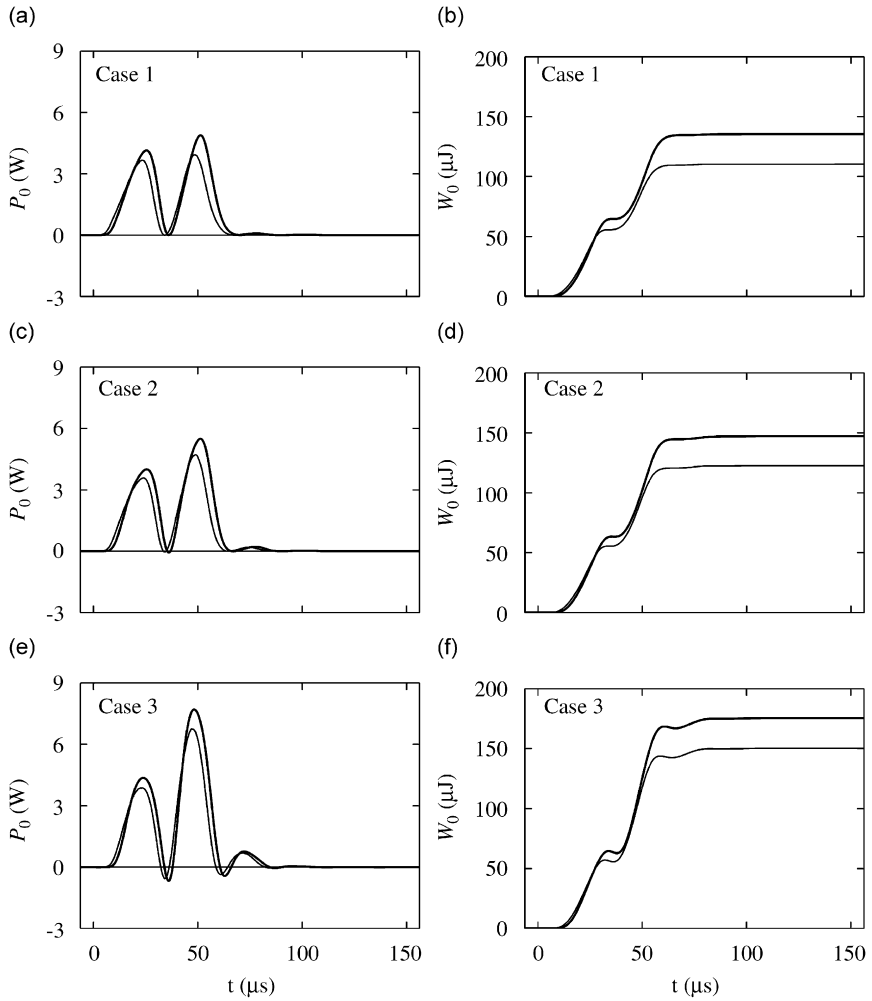

Fig. 6. Electric power P_0 and energy W_0 delivered to the load versus time t for different load impedances $Z_0 = R_0 + i\omega L_0$. (a) Power and (b) energy for Case 1. (c) Power and (d) energy for Case 2. (e) Power and (f) energy for Case 3. Comparison between theoretical (thick curves) and experimental (thin curves) results.

likely that the deviations between theoretical and experimental results for the strains, the voltage, the current, the power, and the energy can be largely explained by the exclusion of such phenomena in the modeling of the laminated PBE and the bar. In addition, they may be partially explained by inaccuracies in geometrical dimensions, material parameters, and measurements.

5. Conclusions

The main conclusions of this study can be summarized as follows: (i) The theoretical and experimental results for the reflected and transmitted strain waves agree quite well; generally, the experimental strain amplitudes are a few percent lower than the theoretical ones. (ii) The changes in load impedance had little effect on the waves. (iii) The voltage and current generated are oscillatory with rapidly decaying tails. (iv) The theoretical and experimental results for voltage and current generally agree well although the experimental peaks are typically 6–11% lower than the theoretical ones. (v) The changes in load impedance had noticeable effect on the voltage and current. (vi) There is a fair overall agreement between the theoretical and experimental results for the electrical power and energy delivered to the load although the experimental power peaks and energy levels are typically 12–19% lower than the corresponding theoretical values. (vii) The

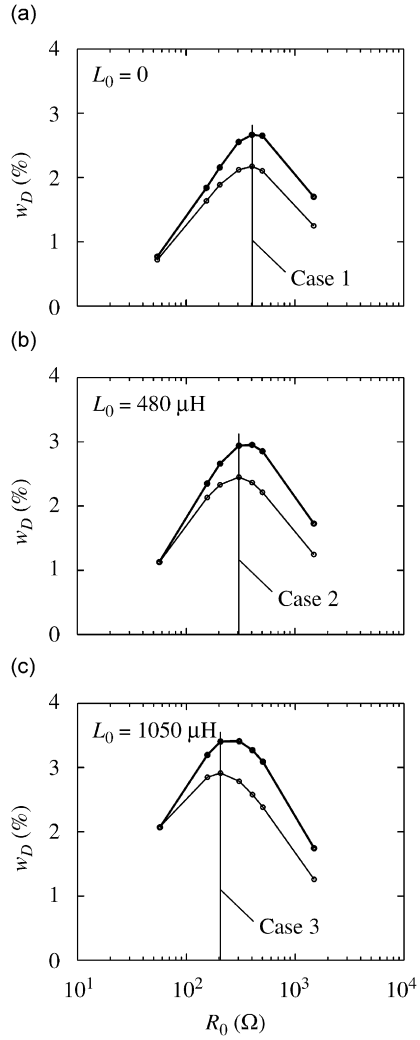

Fig. 7. Relative energy dissipation w_D versus resistive part R_0 of load impedance $Z_0 = R_0 + i\omega L_0$ for load inductance (a) $L_0 = 0$, (b) $L_0 = 480\,\mu H$, and (c) $L_0 = 1050\,\mu H$. Comparison between theoretical (thick curves) and experimental (thin curves) results.

changes in load impedance had significant effect on the power and energy delivered to the load. (viii) The theoretical maxima in relative energy dissipation are about 15–18% lower than the theoretical ones. (ix) Due to impedance mismatch, these maxima around 3% are much lower than the theoretical maximum of 50% for a harmonic wave under condition of impedance match. (x) The experimental results indicate losses in the range 5–10% in the PBE and the external parts of the bars that have not been taken into account theoretically. (xi) Viscoelastic shear in the bonding layers, dielectric losses in the piezoelectric members and generation of bending waves in the external parts of the bar are possible explanations of such losses. (xii) The deviations between theoretical and experimental results may be largely explained by the exclusion of such phenomena in the modeling of the PBE and the bar. They may also be partially explained by inaccuracies in the geometrical dimensions, in the material parameters and in the measurements.

Acknowledgment

The authors gratefully acknowledge the economical support they have received from the Swedish Research Council (Contract no. 621-2001-2156).

References

[1] G. Gautschi, *Piezoelectric Sensorics*, Springer, Berlin/Heidelberg, 2002.
[2] R.M. Lec, Piezoelectric biosensors: recent advances and applications, *IEEE International Frequency Control Symposium and PDA Exhibition*, 2001.
[3] J.K. Dürr, R. Honke, M. von Alberti, R. Sippel, Development of an adaptive lightweight mirror for space application, *Smart Materials and Structures* 12 (2003) 1005–1016.
[4] K.K. Tan, S.C. Ng, S.N. Huang, Assisted reproduction system using piezo actuator. *2004 International Conference on Communications, Circuits and Systems (IEEE Cat. No.04EX914)*, Vol. 2, part 2, 2004, pp. 1200–1203.
[5] T. Ikeda, *Fundamentals of Piezoelectricity*, Oxford University Press, New York, 1990.
[6] E.F. Crawley, J. de Luis, Use of piezoelectric actuators as elements of intelligent structures, *AIAA Journal* 25 (10) (1987) 1373–1385.
[7] J. Pan, C.H. Hansen, S.D. Snyder, A study of the response of a simply supported beam to excitation by a piezoelectric actuator, *Journal of Intelligent Material Systems and Structures* 3 (1) (1992) 3–16.
[8] N.W. Hagood, W.H. Chung, A. von Flotow, Modelling of piezoelectric actuator dynamics for active structural control, *Journal of Intelligent Material Systems and Structures* 1 (3) (1990) 327–354.
[9] R.P. Thornburgh, A. Chattopadhyay, Simultaneous modeling of mechanical and electrical response of smart composite structures, *AIAA Journal* 40 (8) (2002) 1603–1610.
[10] R.P. Thornburgh, A. Chattopadhyay, A. Ghoshal, Transient vibration of smart structures using a coupled piezoelectric-mechanical theory, *Journal of Sound and Vibration* 274 (2004) 53–72.
[11] R. Forward, Electronic damping of vibrations in optical structures, *Journal of Applied Optics* 18 (1979) 690–697.
[12] N.W. Hagood, A. von Flotow, Damping of structural vibrations with piezoelectric materials and passive electrical networks, *Journal of Sound and Vibration* 146 (1991) 243–268.
[13] O.M. Fein, L. Gaul, On the application of shunted piezoelectric material to enhance structural damping of a plate, *Journal of Intelligent Material Systems and Structures* 15 (2004) 737–743.
[14] M. Panella, G. Martinelli, RC distributed circuits for vibration damping in piezo-electromchanical beams, *IEEE Transactions on Circuits and Systems—II: Express Briefs* 52 (8) (2005) 486–490.
[15] G.A. Lesieutre, Vibration damping and control using shunted piezoelectric materials, *The Shock and Vibration Digest* 30 (1998) 187–195.
[16] J. Tang, Y. Liu, K.W. Wang, Semiactive and active-passive hybrid structural damping treatments via piezoelectric materials, *The Shock and Vibration Digest* 32 (2000) 189–200.
[17] S.O. Reza Moheimani, A survey of recent innovations in vibration damping and control using shunted piezoelectric transducers, *IEEE Transactions on Control Systems Technology* 11 (4) (2003) 482–494.
[18] S. Hurlebaus, L. Gaul, Smart structure dynamics, *Mechanical Systems and Signal Processing* 20 (2006) 255–281.
[19] A. Jansson, B. Lundberg, Three-port impedance model of a piezoelectric bar element: application to generation and damping of extensional waves, *Journal of Sound and Vibration* (2008) accepted for publication.
[20] A. Jansson, U. Valdek, B. Lundberg, Generation of prescribed waves in an elastic bar by use of piezoelectric actuators driven by a linear power amplifier, *Journal of Sound and Vibration* 306 (2007) 751–765.